ANL/MSD/CP--84416
Conf-9503144--1

# Structure and Properties of Heteroepitaxial $Pb(Zr_{0.35}Ti_{0.65})O_3/SrRuO_3$ Multilayer Thin Films on $SrTiO_3(100)$ Prepared by MOCVD and RF Sputtering*

C. M. Foster, R. Csencsits, G. R. Bai, and Z. Li
*Materials Science Division*
*Argonne National Laboratory, Argonne, IL 60439*

L. A. Wills and R. Hiskes
*Hewlett-Packard Laboratories, Hewlett-Packard Company, Palo Alto, CA*

H. N. Al-Shareef and D. Dimos
*Sandia National Laboratory, Albuquerque, NM*

April 1995



Presented at the 7th International Symposium on Integrated Ferroelectrics, Colorado Springs, CO, March 20-22, 1995; to be published in the Proceedings.

*Work at ANL was supported by the U.S. Department of Energy, Basic Energy Sciences-Materials Science, under contract #W-31-109-ENG-38 under the joint CRADA with Hewlett-Packard Company #C9301701; work at Sandia National Laboratory was supported by the U.S. DOE under contract #DE-AC04-94AL85000.

# STRUCTURE AND PROPERTIES OF HETEROEPITAXIAL $Pb(Zr_{0.35}Ti_{0.65})O_3/SrRuO_3$ MULTILAYER THIN FILMS ON $SrTiO_3(100)$ PREPARED BY MOCVD AND RF SPUTTERING

C. M. FOSTER, R. CSENCSITS, G. R. BAI, AND Z. LI
Materials Science Division, Argonne National Laboratory, Argonne, IL, USA

L. A. WILLS AND R. HISKES
Hewlett Packard Laboratories, Hewlett-Packard Company, Palo Alto, CA, USA

H. N. AL-SHAREEF AND D. DIMOS
Sandia National Laboratory, Albuquerque, NM, USA

## ABSTRACT

Epitaxial $SrRuO_3$ thin films were deposited on $SrTiO_3(100)$ substrates by RF sputtering for use as bottom electrodes and epitaxial buffer layers. On these conductive substrates, epitaxial $Pb(Zr_{0.35}Ti_{0.65})O_3$ (PZT) thin films were deposited by metalorganic chemical vapor deposition (MOCVD). X-ray diffraction (XRD), transmission electron microscopy (TEM) and optical waveguiding were used to characterize the phase, refractive index, and film thickness of the deposited films. The epitaxial PZT films were c-axis oriented and contained ~19.7% volume fraction of 90° domains. Ferroelectric hysteresis and dielectric measurements of epitaxial PZT ferroelectric capacitor structures formed using sputtered ITO top electrodes showed: a remanent polarization of 51.8 $\mu C/cm^2$, a coercive field of 54.9 kV/cm, a dielectric constant of 410, a bipolar resistivity of ~$5.8 \times 10^9$ Ω-cm at a field of 275 kV/cm, and a breakdown strength of >400 kV/cm. The cyclic fatigue behavior of the films showed a strong dependence on the choice of electrode materials and the fatiguing wave form. These data support the model that the fatigue mechanism in these films arises from the trapping of injected charge carriers and is predominately an electronic phenomenon.

## INTRODUCTION

Current interest in ferroelectric thin films results from the numerous potential applications for these materials which utilize the unique dielectric, pyroelectric, electro-optic, acousto-optic, and piezo-electric properties of ferroelectrics materials[1]. The

synthesis of thin films of the lead-based ferroelectrics, $PbTiO_3$, $Pb(Zr_xTi_{1-x})O_3$ (PZT), $(Pb_{1-x}La_x)(Zr_yTi_{1-y})O_3$ (PLZT), etc., using a variety of techniques (i. e., sol-gel, sputtering, laser ablation, MOCVD) and the resulting properties of the films have been studied extensively[1]. For many applications, such as non-volatile dynamic random access memory (DRAM) or electro-optic waveguide modulators, a highly textured microstructure is preferable or essential. Ferroelectric film deposition using MOCVD has been widely reported and has been shown to be able to produce film microstructures from random polycrystalline to highly epitaxial[2]. Devices fabricated from single-crystal films with low defect density could potentially take full advantage of the tensor nature of the anisotropic properties of ferroelectric materials, resulting in improved device performance and enhanced device characteristics. In addition, for applications such as optical waveguide modulators, waveguide frequency doublers and Surface Acoustic Wave (SAW) delay lines, the high degree of structural perfection in such epitaxial films could substantially reduce propagation losses associated with grain boundary scattering to levels where the total insertion losses are sufficiently low (i. e., <1.0 dB/cm) for feasible device applications.

We have systematically studied the effects of gas-phase composition, substrate materials, substrate orientation, and deposition temperature on the phase, composition, crystallinity, morphology and domain structure of epitaxial thin films of $PbTiO_3$[3-5]. We have also discussed the effects of the choice of substrate material on the crystallinity, microstructure, domain formation, defect structure and optical properties of $PbTiO_3$ thin films[6-7]. In this paper, we report results on the growth, characterization and properties of $Pb(Zr_{0.35}Ti_{0.65})O_3$ thin films deposited on $SrRuO_3$ buffered $SrTiO_3(100)$ substrates using MOCVD.

## EXPERIMENTAL

Epitaxial $SrRuO_3$ thin films were deposited on epitaxial-grade (100) $SrTiO_3$ substrates by 90° off-axis, RF magnetron sputtering at a growth pressure of 15 Pa and deposition temperature of 650°C. Sputter deposition commenced at a power of 60W and a $Ar/O_2$ flow rate of 120/80 sccm. The growth rate of the $SrRuO_3$ layers was estimated from RBS to be ~160Å per hour[8].

PZT thin film depositions were carried out in a low pressure, horizontal, cold wall reactor with a resistive substrate heater. The $SrRuO_3$ buffered $SrTiO_3(100)$ were used as the substrate material. Tetraethyl lead, $Pb(C_2H_5)_4$, zirconium t-butoxide, $Zr(OC(CH_3)_3)_4$, and titanium isopropoxide, $Ti(OC_3H_7)_4$, (Morton International, Advanced Materials, Danvers, MA) were chosen as the metal ion precursors. UHP (99.9995%) $N_2$ and $O_2$ were used as the carrier gas and the oxidant, respectively. Details of the reactor design and deposition methods have been previously reported[3-7,9]. The growth conditions for the deposition of $Pb(Zr_{0.65}Ti_{0.35})O_3$ are shown in Table I.

The crystallinity, domain structure and chemical composition of the $Pb(Zr_{0.35}Ti_{0.65})O_3$ films were investigated with x-ray diffraction (XRD) analysis. The chemical composition was verified using energy-dispersive x-ray analysis. X-ray θ-2θ diffraction and θ-rocking scans of the films were obtained using a Rigaku diffractometer and a 15 kW $Cu_{K\alpha}$ rotating anode x-ray source. Prism-coupling waveguide experiments were performed with a Metricon 2010 Prism-Film coupler using a HeNe laser (632.8

nm); this system has been described elsewhere[9]. Descriptions of the TEM sample preparation and methods have been previously reported[3-4]. Ferroelectric hysteresis, bipolar resistance, dielectric fatigue, and dielectric breakdown measurement were obtained using a Radiant Technologies RT66A tester.

TABLE I. GROWTH CONDITIONS

| | |
|---|---|
| Substrate temperature | 700°C |
| Reactor pressure | 8 torr |
| OM precursor temperature | $Ti(OC_3H_7)_4$ - 39-40 °C<br>$Pb(C_2H_5)_4$ - 27-28 °C<br>$Zr(OC(CH_3)_3)_4$ - 29-30 °C |
| OM precursor pressure | $Ti(OC_3H_7)_4$ - 37 torr<br>$Pb(C_2H_5)_4$ - 150 torr<br>$Zr(OC(CH_3)_3)_4$ - 400 torr |
| Flow rate of reactant gas ($O_2$) | 200 sccm |
| Flow rate of OM and carrier gas ($N_2$)<br>$Pb(Zr_{0.35}Ti_{0.65})O_3$ | $Ti(OC_3H_7)_4$ - 35 sccm<br>$Pb(C_2H_5)_4$ - 50 sccm<br>$Zr(OC(CH_3)_3)_4$ - 25 sccm |
| Flow rate of background gas ($N_2$) | 600 sccm |
| Film thickness | 0.2-1.0 μm |
| Film growth rate | 40 Å/min. |
| Substrates | $SrRuO_3/SrTiO_3$ (100) |

## RESULTS AND DISCUSSION

Epitaxial metallic oxide layers have been show to yield enhanced device performance due to their excellent chemical and structural compatibility with many oxide materials[10]. The growth of $SrRuO_3$ and other conductive oxide thin films for use as buffer layers and epitaxial electrodes has shown great promise in the field of integrated ferroelectrics because of the significant improvement in fatigue characteristic of capacitors formed using these electrodes[11]. We have used epitaxial $SrRuO_3$(001) thin films deposited on $SrTiO_3$(100) by RF sputtering as bottom electrodes and deposited epitaxial $Pb(Zr_{0.35}Ti_{0.65})O_3$ thin films on these films by MOCVD. Using the growth conditions specified in Table I, the films produced were pure perovskite phase with a single-crystalline structure. Shown in Fig. 1 is the XRD data for the $Pb(Zr_{0.35}Ti_{0.65})O_3$ films deposited on epitaxial $SrRuO_3$(100) buffered $SrTiO_3$(100). The $\theta$–$2\theta$ scan, the $\theta$-rocking for the PZT(002) reflection and the $\theta$-rocking for the PZT(200) reflection are shown in Fig. 1a, 1b and 1c, respectively. From the $\theta$-$2\theta$ scan, we determine that the films have a nominal composition of $Pb(Zr_{0.35}Ti_{0.65})O_3$ and are highly *c*-axis oriented. We have previously demonstrated that the presence of the PZT(35/65) (100) reflection in the $\theta$-$2\theta$ scans results from the presence of 90° domains (*a*-axis) in the films[6]. In addition, the films are epitaxial grown with respect to both the $SrRuO_3$ layer and the substrate. We have previously shown that the a volume fraction of 90° domains in epitaxial PZT thin films can be determined directly from the integrated intensity ratio of

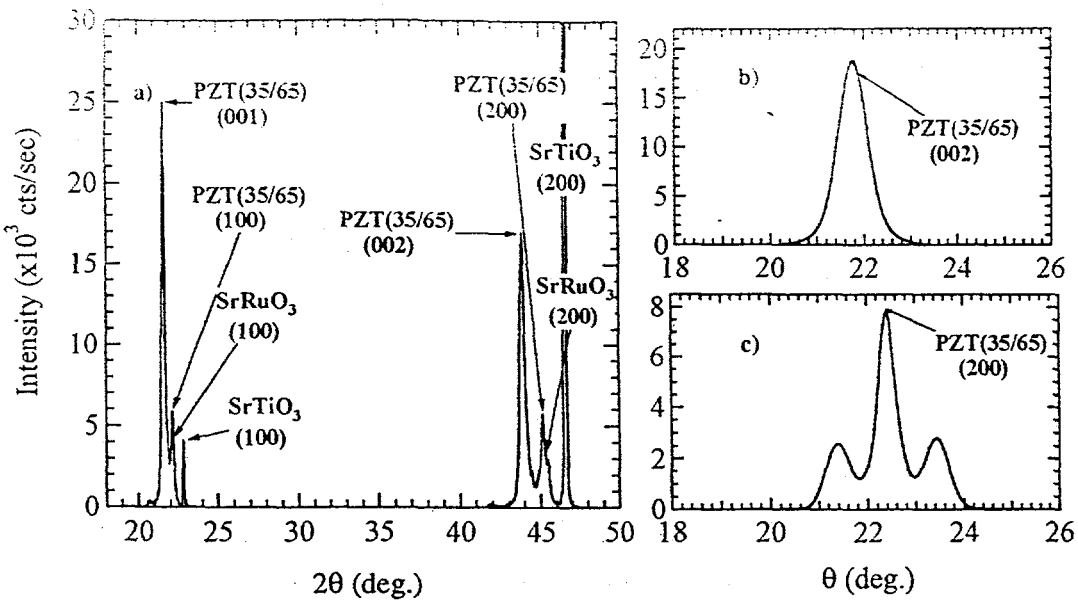


Figure 1. XRD data for a $Pb(Zr_{0.35}Ti_{0.65})O_3$ films grown on epitaxial $SrRuO_3(100)$ buffered $SrTiO_3(100)$. The θ–2θ scan, the θ-rocking for the PZT(002) reflection and the θ-rocking for the PZT(200) reflection are shown in Fig. 2a, 2b and 2c, respectively.

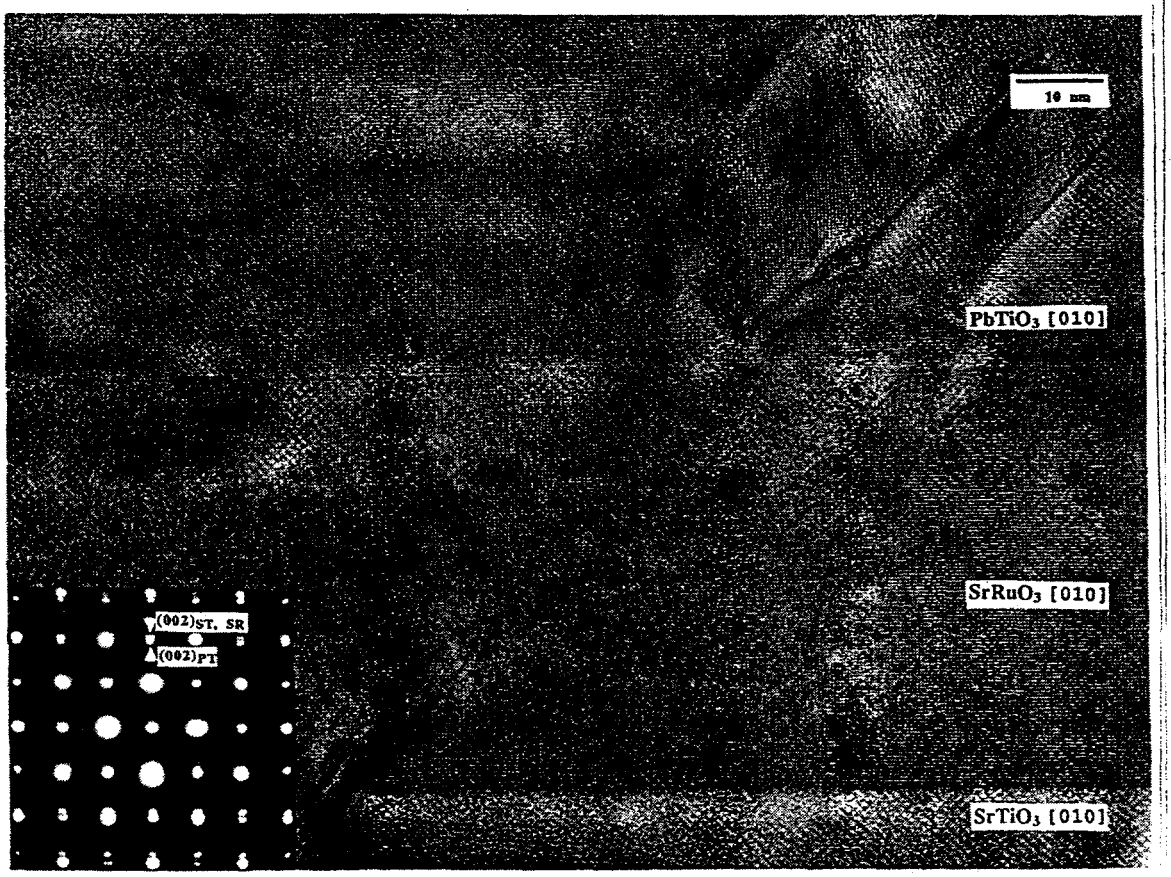


Figure 2. High resolution cross-sectional TEM image of the $PbTiO_3(001)$ / $SrRuO_3(100)$ / $SrTiO_3(100)$ interfaces showing that the individual layer interfaces are atomically sharp. The dominate defects in the film are 90° domains and threading dislocations. The inset shows the selected area electron diffraction pattern of the interface region.

the PZT (002) and (200) reflections[12]; for these films we determine that the films contain a volume fraction of 90° domains of ~19.7%.

To illustrate the quality of the interfacial structure obtained using epitaxial $SrRuO_3$ buffer layers, we show in Fig. 2 the cross-section TEM image of a $PbTiO_3(001)/SrRuO_3(100)/SrTiO_3(100)$ epitaxial film. The image shows that the films is epitaxial *c*-axis oriented, with 90° domains and threading dislocations being the primary structural defects. The thickness of the $SrRuO_3$ layer is ~470Å. Note that the 90° domain visible in the image clearly nucleates at structural defects in the substrate. The strain contrast associated with the substrate defect site appears to propagate directly through the $SrRuO_3$ layer into the $PbTiO_3$ layer. In addition, in lower magnification images, we observed threading dislocations that appear normal to the substrate/film interface and propagate through the 90° domains. Presumably, this would indicate that these dislocations form prior to the ferroelectric phase transition while the films are in the cubic state. The $PbTiO_3(001)/SrRuO_3(100)/SrTiO_3(100)$ interfaces shown in Fig. 2 are atomically sharp; note that the $PbTiO_3(001)/SrRuO_3(100)$ interface appears to be cleaner that the $SrRuO_3(100)/SrTiO_3(100)$ interface indicating that the deposition of the buffer layer appears to improve the quality of the substrate surface resulting in an improved ferroelectric film. The selected area electron diffraction pattern of the interface structure is shown as a inset to Fig. 2. From this pattern, we determined the epitaxial relationships between the $PbTiO_3$ and $SrRuO_3$ films and the $SrTiO_3$ substrate: $(100)[010]PbTiO_3//(100)[010]SrRuO_3//(100)[010]SrTiO_3$.

Optical waveguiding experiments showed that the $Pb(Zr_{0.35}Ti_{0.65})O_3(001)$ film had an ordinary refractive index of 2.5814 at 632.8 nm. These measurements directly determined the thickness of each film and showed that the growth rate for the films was consistently ~40Å/min. for each run.

To characterize the ferroelectric properties of the films, ITO glass top electrodes were RF sputter deposited through a shadow mask to form capacitor structures on the $Pb(Zr_{0.35}Ti_{0.65})O_3/SrRuO_3(100)/SrTiO_3(100)$ films. Shown in Fig. 3 are the results of

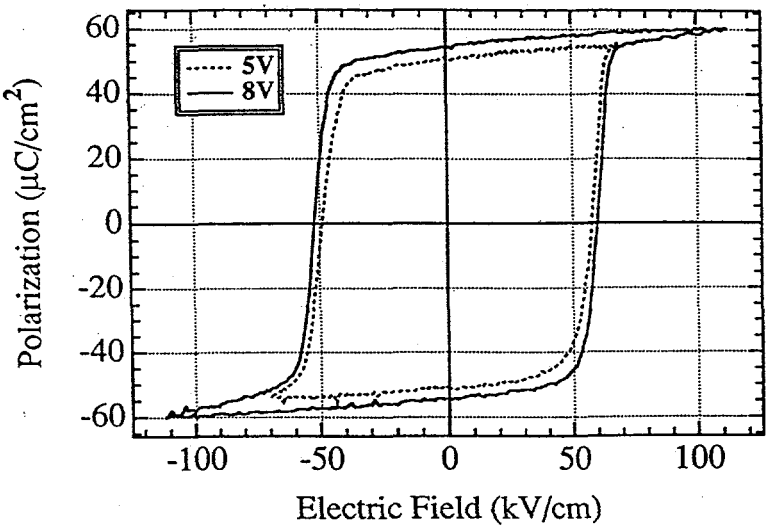


Figure 3. The ferroelectric polarization hysteresis loops (P-E curves) for an ITO / PZT(35/65) (001) / $SrRuO_3(100)$ / $SrTiO_3$ (100) capacitor at maximum applied voltages of 5V and 8V; the PZT film thickness was 7166Å.

polarization hysteresis loops (P-E curves) for an ITO / PZT(35/65) (001) / $SrRuO_3$(100) /$SrTiO_3$ (100) capacitor at maximum applied voltages of 5V and 8V; the PZT film thickness was 7166Å. The loops are quite square and well saturated at 8V. The results of these measurement are: a remanent polarization of 52.8 $\mu C/cm^2$, a saturation polarization of 57.9 $\mu C/cm^2$, a coercive field of 55.9 kV/cm, and a bipolar resistivity of $>5.8x10^9$ Ω-cm at 275 kV/cm. The dielectric breakdown strength of this capacitor was >400kV/cm (this field strength was the limit of our instrument). The dielectric constant of this films at 1 MHz was 410. The electrical measurements indicate that the properties of this film are a significant fraction of those of bulk material (e. g., ~85% of the single crystal remanent polarization). However, we measured a volume fraction of 90° domains of ~19%. In-situ XRD measurements of the film under saturation bias indicate that no portion of this twin volume undergoes 90°. This shows that this volume volume fraction of the film can not contribute to the measured remanent polarization and effectively reduces the measured capacitor area by ~12%; consequently, the true remanent polarization should be as high as ~62.6 $\mu C/cm^2$, very close to that of the bulk material at this composition.

Ferroelectric polarization fatigue tests were performed on these capacitors using 10 kHz triangular, square, and sinusoidal wave forms at ±8V. The results of these measurements are shown in Fig. 4, and are plotted as the changes in the net switched remanent polarization charge ($P_r^*$-$P_r^\wedge$), which is the difference between the switched and non-switched remanent polarization. The fatigue curves for square and sinusoidal wave forms are similar and showed significant polarization fatigue, with the greater fatigue occurring while using the square wave form. In comparison, the fatigue curves obtained using the triangle wave form showed little polarization fatigue out to $10^9$ cycles. In Fig. 5, we show the hysteresis loops before and after the fatigue tests for each of the wave forms. Note that for all the wave forms, the squareness of the loops is maintained after fatigue. In addition, for the triangular and sinusoidal wave forms, there is no change in the coercive voltages while for the square wave form, the coercive voltage decreases.

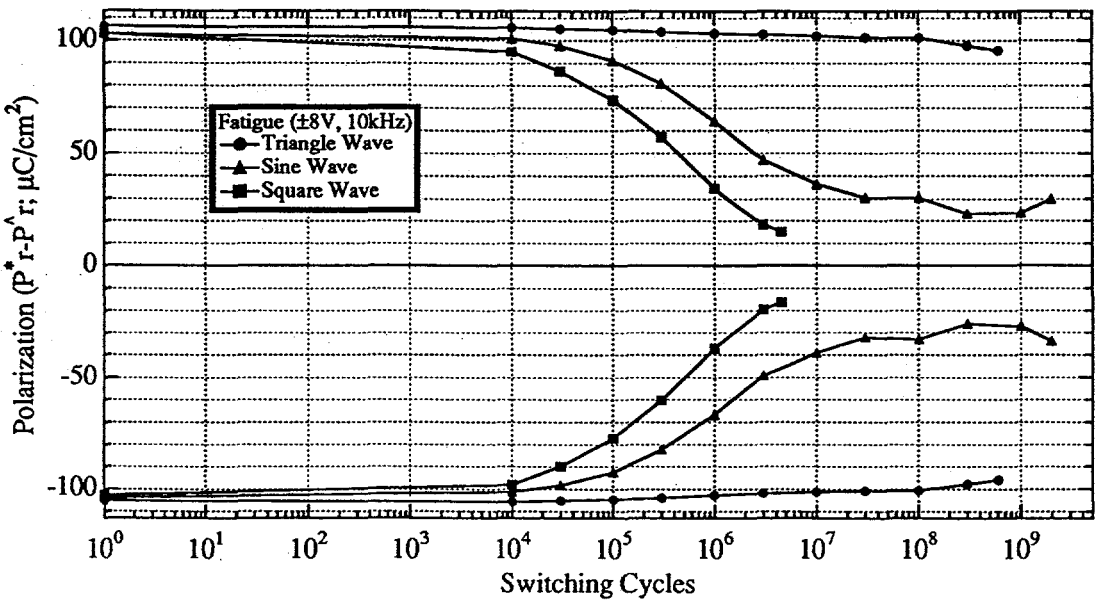


Figure 4. Ferroelectric polarization fatigue measurements performed on an ITO/ PZT(35/65) (001)/$SrRuO_3$(100)/$SrTiO_3$(100) capacitor using 10 kHz triangular, square, and sinusoidal wave forms at ±8V; the PZT film thickness was 7166Å.

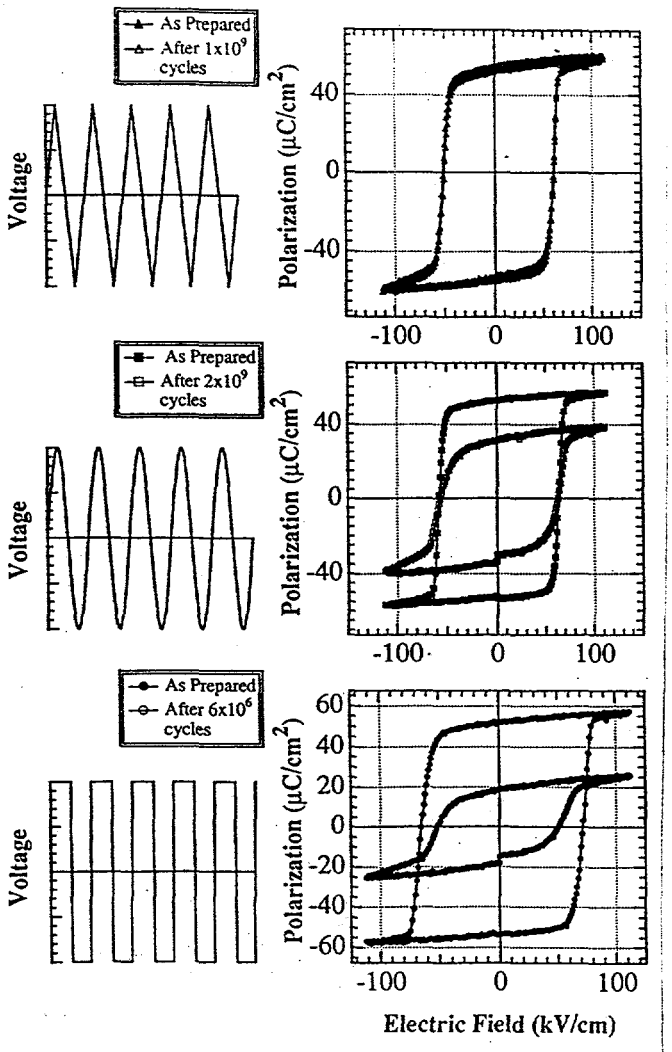


Figure 5. Hysteresis loops (before and after fatigue) illustrating the wave form dependence of the polarization fatigue (10 kHz ±8V) of an ITO/PZT(35/65) (001)/ $SrRuO_3$(100)/$SrTiO_3$ (100) capacitor; the PZT film thickness was 7166Å.

For the case of fatigue with a triangular wave form, we observed a maximum of ~20% polar fatigue. However, the hysteresis loops measured at the end of the fatigue tests were essentially the same as the loops prior to fatigue. Therefore, the degradation of the polarization properties of the sample is rejuvenated during the hysteresis loop measurement at the end of the fatigue test. To confirm that the observed fatigue is genuine, we measured the recovery of the remanent polarization of the sample by performing hysteresis loop measurements on a fatigued capacitor at gradually increasing voltages, and then compared these loops to hysteresis loops taken under the same voltages prior to the fatigue test. These data are shown in Fig. 6.: the remanent and saturation polarizations measured after fatigue become increasingly close in magnitude to their values prior to fatigue as the measuring voltage is increased. This suggests that the polarization fatigue observed when using a triangular wave form can be rejuvenated using a voltage equal to its saturation voltage.

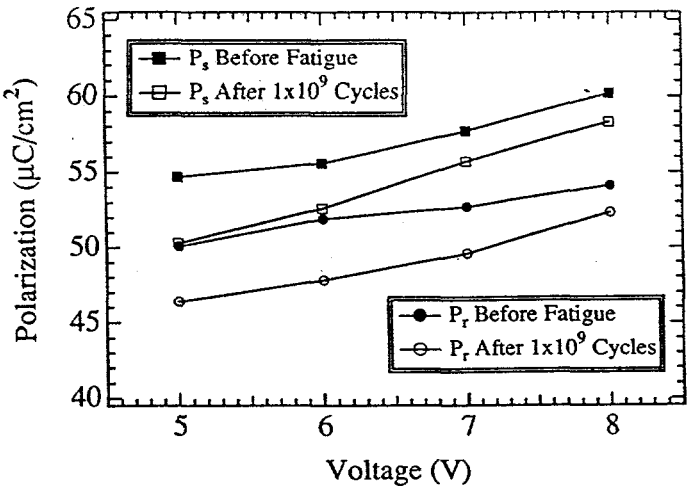


Figure 6. Recovery of the ferroelectric polarization hysteresis loops (P-E curves) after fatigue for an ITO/PZT(35/65) (001)/$SrRuO_3$(100)/$SrTiO_3$(100) capacitor with increasing measuring voltage; the PZT film thickness was 7166Å.

For the three fatiguing wave forms, the rate of fatigue increases significantly with the length of time that the capacitor is subjected to a saturation voltage. If the fatigue is caused by an internal space charge field resulting from the trapping of injected electronic charge carriers at either point defects or domain walls[13], then the rate of fatigue should increase as the number of charge carriers injected per switching cycle is increased. Since the number of charge carriers injected from the electrodes into the sample is proportional to the length of time at the saturation voltage, then the wave-form dependence of the fatigue in these films strongly favors an electronic origin of the fatigue.

While the exact mechanism for the wave form dependence of the fatigue is not completely certain, it should be noted that when capacitors prepared with sol-gel deposited PZT of the form Pt/PZT/Pt/Ti/$SiO_2$/Si were subjected to similar fatigue tests using triangular, square and sinusoidal wave forms, significant fatigue was observed in all three cases. This indicates that the minimal fatigue observed in the MOCVD prepared capacitors using triangular wave forms is not observed in all types of PZT capacitors. There are two important differences between these two types of capacitors. First, the sol-gel produced Pt/PZT/Pt/Ti/$SiO_2$/Si materials are polycrystalline, while the MOCVD produced ITO/PZT/$SrRuO_3$/$SrTiO_3$ materials are highly oriented. Thus there is more stress associated with the switched state in the polycrystalline sol-gel materials than in the highly-oriented MOCVD materials since for highly oriented films it is likely that 90° domains are strongly pinned; this is evident from the squareness of the hysteresis loops for the MOCVD samples. Second, the MOCVD sample has conducting oxide electrodes while the sol-gel sample has Pt electrodes. From these differences alone, the wave-form dependence of the fatigue for the MOCVD samples could arise from three sources: 1) an effect of extreme sample orientation, 2) an effect of oxide electrodes, or 3) an effect specific to the ITO top electrode itself. In addition, there are differences in grain size, domian size and 90° domain population between the two types of samples that could play a role. In order investigate these effects, wave-form dependent fatigue tests were performed on a sol-gel prepared polycrystalline $RuO_2$/PZT(36/65)/$RuO_2$/Si capacitor. In this case, significant fatigue was observed for all wave forms. Thus, the presence of

oxide electrodes by themselves is not the origin of this effect. Further experiments are needed are currently underway. In particular, we are investigating the wave-form dependence of the fatigue for MOCVD produced capacitors with both polycrystalline and epitaxial $(La_{0.5}Sr_{0.5})CoO_3$ and $SrRuO_3$ top electrodes.

We note that the MOCVD growth conditions for these PZT films have not been optimized and, in principle, improvements in the films crystallinity and properties could be achieved. These results indicate that through the use of epitaxial buffer layers and electrode materials, very high structural perfection can be achieved with commensurate bulk-like properties in epitaxial ferroelectric films.

## ACKNOWLEDGMENTS

The work at Argonne National Laboratory was supported by the U. S. Department of Energy, Basic Energy Science-Materials Science through contract #W-31-109-ENG-38 under the joint CRADA with Hewlett-Packard Company #C9301701. TEM analysis was carried out at the Electron Microscopy Center for Materials Research at Argonne National Laboratory. The work at Sandia National Laboratory was supported by the U. S. Department of Energy under contract #DE-AC04-94AL85000.

## REFERENCES

1. For example see, Ferroelectric Thin Films III, ed. E. R. Myers, B. A. Tuttle, S. B. Desu, and P. K. Larsen, (Mat. Res. Soc. Symp. Proc. Vol. 310, San Francisco, CA 1993).
2. C. J. Brierley, C. Trundle, L. Considine, R. W. Whatmore, and F. W. Ainger, Ferroelectrics, 90, 181 (1989); A. I. Kingon, K. Y. Hsieh, L. L. King, S. H. Rou, K. J. Backmann, and R. F. Davis, in Ferroelectric Thin Films, ed. by E. R. Myers and A. I. Kingon, (Mat. Res. Soc. Symp. Proc. Vol. 200, Pittsburg, PA 1990); T. Katayama, M. Fuzimoto, M. Shimizu, and T. Shiosaki, Jpn. J. Appl. Phys., 30, 2189 (1991).
3. G. R. Bai, H. L. M. Chang, H. K. Kim, C. M. Foster, and D. J. Lam, Appl. Phys. Lett., 64, 408 (1992); Y. Gao, G. Bai, K. L. Merkle, Y. Shi, H. L. M. Chang, Z. Shen, and D. J. Lam, J. Mater. Res., 8, 145 (1993).
4. G. R. Bai, H. L. M. Chang, C. M. Foster, Z. Shen, and D. J. Lam, J. Mater. Res., 9, 156 (1994).
5. H. You, H. L. M. Chang, R. P. Chiarello, and D. J. Lam, in Heteroepitaxy of Dissimilar Materials, ed. by R. F. C. Ferrow, J. P. Harbison, P. S. Peercy, and A. Zangwill (Mat. Res. Soc. Symp. Proc. Vol. 221, Pittsburg, PA 1990) p. 181.
6. C. M. Foster, Z. Li, G. R. Bai, H. You, D. Guo, and H. L. M. Chang, in Epitaxial Oxide Thin Films and Heterostructures, ed. D. K. Fork, J. M. Phillips, R. Ramesh, and R. M. Wolf, (Mat. Res. Soc. Symp. Proc. Vol. 341, San Francisco, CA 1994).
7. C. M. Foster, Z. Li, M. Buckett, D. Miller, P. M. Baldo, L. E. Rehn, G. R. Bai, D. Guo, H. You and K. L. Merkle, (J. Appl. Phys. in press).
8. L. A. Wills and J. Amano, in Ferroelectric Thin Films IV, presented at the 1994 Fall MRS Meeting, Boston, MA 1994.
9. C. M. Foster, S.-K. Chan, H. L. M. Chang, R. P. Chiarello, T. J. Zhang, J. Guo, and D. J. Lam, J. Appl. Phys., 73, 7823 (1993).

10. C. B. Eom, J. M. Phillips and R. J. Cava, in Epitaxial Oxide Thin Films and Heterostructures, ed. D. K. Fork, J. M. Phillips, R. Ramesh, and R. M. Wolf, (Mat. Res. Soc. Symp. Proc. Vol. 341, San Francisco, CA 1994).
11. H. N. Al-Shareef, A. I. Kingon, X. Chen, K. R. Bellur, and O. Auciello, J. Mater. Res., 9 (11), 2968 (1994).
12. C. M. Foster, Z. Li, M. Buckett, D. Miller, P. M. Baldo, L. E. Rehn, G. R. Bai, D. Guo, H. You, and K. L. Merkle, J. Appl. Phys., in press.
13. W. L. Warren, D. Dimos, B. A. Tuttle, R. D. Nasby, and G. E. Pike, Appl. Phys. Lett., 65 (8), 1018 (1994).